

Title: **Microscopical Examination
of Plastic-Bonded Explosives**

Author(s): Cary B. Skidmore
David S. Phillips
Nathan B. Crane

Submitted to:

<http://lib-www.lanl.gov/la-pubs/00412752.pdf>



Los Alamos
NATIONAL LABORATORY

Los Alamos National Laboratory, an affirmative action/equal opportunity employer, is operated by the University of California for the U.S. Department of Energy under contract W-7405-ENG-36. By acceptance of this article, the publisher recognizes that the U.S. Government retains a nonexclusive, royalty-free license to publish or reproduce the published form of this contribution, or to allow others to do so, for U.S. Government purposes. The Los Alamos National Laboratory requests that the publisher identify this article as work performed under the auspices of the U.S. Department of Energy. Los Alamos National Laboratory strongly supports academic freedom and a researcher's right to publish; therefore, the Laboratory as an institution does not endorse the viewpoint of a publication or guarantee its technical correctness.

Microscopical Examination of Plastic-Bonded Explosives

by
Cary B. Skidmore, David S. Phillips, and Nathan B. Crane
Los Alamos National Laboratory
Los Alamos, New Mexico 87545

Abstract

Polarized Light Microscopy is a powerful technique for the identification of powdered explosives. We apply the technique here to the characterization in bulk of composite, plastic-bonded explosives, typically consisting of 95 w/o explosive particulate and 5 w/o polymeric binder. Mounting and polishing techniques are described, along with attendant issues of mount or binder dyeing and some complications of cleaning very soft samples. The microstructures of PBX 9501 (based on cyclotetramethylene tetranitramine, or HMX), PBX 9502 (based on triaminotrinitrobenzene or TATB), and X-0535 (based on diaminotetrazine dioxide, or TZX) are compared and contrasted. Selected case studies are presented in which development of prominent structural characteristics, such as particle size and crack density, are tracked from the starting powders through formulation and pressing to serviceable, formed articles.

Introduction

Polarized Light Microscopy has been used historically to characterize explosives such as RDX, HMX, and TNT in their crystalline form. A newer generation of explosives including TATB and TZX have not been studied as thoroughly by this method. These explosives are typically made into useful components by mixing with a few volume percent polymeric binder (which greatly increases the mechanical integrity of the finished article), pressing, and machining to shape. The post World War II generation of HMX-based explosives also use polymeric binders (in contrast to older compositions typically melt cast with TNT). The new compositions developed by Los Alamos National Laboratory are designated Plastic-Bonded Explosives (PBXs). A typical formulation process is to slurry the powdered explosive in water, add a solution of binder dissolved in solvent, then draw off the solvent with vacuum and/or heat. The surface energies of the materials are such that the binder clings to the explosive crystallites rather than forming small globules of binder alone. The resulting molding powder is then consolidated through heat and pressure in either an isostatic or hydrostatic pressing operation. Subsequent machining to final shape yields a finished component.

This paper presents techniques for the preparation and examination of PBX samples using Polarized Light Microscopy. Direct observation of particle sizes, intragranular void features, and deformation characteristics at various stages of processing and various levels of insult are important to understanding the micromechanical behavior of these materials. This understanding will be used by others to model in detail the response of explosives to external stimuli.

The three compositions used in this study were chosen for their qualitative differences within the class of PBXs that uses only a few percent binder. PBX 9501 is made from a 3:1 mix of coarse: fine classes of HMX and 7.3 v/o of a binder containing estane (polyurethane) with nitroplasticizer (bisdinitropropyl acetal/formal). The pressed piece used in this study contained only 1 % porosity. PBX 9502 is made from dry-aminated TATB with 4.8 v/o of a Kel-F 800 binder (polychlorotrifluoroethylene). The particle size distribution of TATB in the PBX 9502 formulation is much narrower than of the HMX in PBX 9501. The pressed piece of PBX 9502 use in this study included 3 % porosity. TATB crystals are known to have an abundance of "worm-hole" defects from

the production synthesis process. X-0535 is TZX with 5.4 v/o of Oxy 461 binder (polyvinylchloride copolymer resin) It is an experimental explosive whose synthesis methods are still being optimized, and no specification yet exists for its particle size distribution. The consolidated piece used in this study included 4 % porosity. Qualitatively, HMX is reported to be a more brittle crystal. TATB crystals are soft, mechanically similar to graphite. TZX was reported to be abrasive to machine tools. The present study provides microstructural and micromechanical investigations of these assertions.

Experimental Procedure

Materials

The HMX-based materials examined here were prepared from a commercially produced molding powder (Holston 730-010) in accordance with to Los Alamos specifications for PBX 9501. This powder was then uniaxially die pressed to high density cylindrical parts at 90°C and 20,000 psi, using two cyclic applications of the pressure. The geometric density of the parts was measured after cooling and compared with expectations based on the known formulation and the rule of mixtures. For comparison, two pressed pieces of pure HMX were prepared using laboratory materials simulating the coarse and fine fractions of the specified molding powder formulation. The geometric densities of these pellets indicated 10% porosity for the fine fraction and 7% for the coarse fraction. Finally, one sample of ballistically insulated PBX 9501 was kindly provided by Dr. Blaine W Asay from his suite of experiments measuring strain accumulation by speckle photography¹.

The TATB-based materials were also prepared from a commercial molding powder (Holston 890-007) according to Los Alamos specification for PBX 9502. For the pressed piece, the powder was uniaxially die pressed to 3% porosity at ambient temperature. Another sample form was prepared (lot Holston 890-018) by isostatic pressing to the same porosity at elevated temperature and subsequently introducing cracks by compression testing to failure.

The TZX-based materials were prepared from a locally produced batch of molding powder. As with the other principal samples, the pressed piece was consolidated with heat and pressure in a uniaxial die operation.

Preparation

Sample preparation for microscopical examination was accomplished by traditional metallographic means. Since the materials of interest are by no means traditional metals, a variety of small but significant embellishments on the procedure were developed in the course of this work. Several are described here.

Samples were potted in commercial low-viscosity epoxide mounts with traditional amine hardening agent². Samples were cured in a vessel pressurized 500-1000 psi. For some samples, especially mechanically insulated ones, a fluorescein-based dye was added to the epoxy resin to facilitate identification of crack paths. The amine-cured epoxy medium is not ideally compatible with the explosive materials of interest – it both decreases the temperature of exothermic decomposition measured in differential thermal analysis experiments and it visibly dissolves some components from the 9501 binder system. In the latter experiment, granules, porous pressings, and isolated samples of PBX9501 binder all develop brown stains in the epoxy near its interface with the binder, due to the gradual dissolution of nitroplasticizer from the binder into the epoxy. Both these observations lead us to treat potted mounts with respect, though we have not yet observed hazardous decomposition of any of our samples.

Samples were ground using standard silicon carbide papers (600 and 800 grit American) and modest pressures ($\sim 1 \text{ Nt./cm}^2$ sample) on automated polishing equipment³. In comparison with metallographic tradition, the selection of a 600 grit coarse grinding medium is unusual. This selection, though, is motivated by the exceptionally low toughness of these materials – Palmer and Field⁴, for instance, quote a toughness of $0.05 \text{ MN/m}^{3/2}$ for PBX 9501, four orders of magnitude smaller than typical engineering alloys!

Samples were polished using the oxide slurry method on the same equipment using somewhat larger pressures ($\sim 2 \text{ Nt./cm}^2$). The first stage of such polishing using 1 micron alpha alumina on silk is critically important to remove the gross damage from previous grinding. This stage is extended as needed in five minute increments, until the structure observed becomes perceptibly constant. This surface is then fine polished with 0.3 micron alumina on silk and, briefly, with 0.05 micron colloidal silica on a soft fine sponge-like cloth⁵.

Sample cleaning between polishing stages proved to be difficult, since cotton balls proved hard enough to scratch both HMX and TATB crystals. This was solved by rinsing with water and drying with foam-tipped clean-room swabs.

Analysis

Most of the samples described here were analyzed in reflected light after this preparation. A few were remounted polished side down to a glass slide using the same epoxy, sawed again to remove the majority of the mount, repolished as above, and examined further in transmitted light.

Samples were examined using a Zeiss Axiophot microscope equipped with a Kodak Megaplug 1.4 CCD camera. The camera is C-mounted without transfer optics, providing a pixel resolution about half the Rayleigh limit and thus satisfying the Nyquist criterion near the theoretical resolution of the microscope. High resolution images, where possible, were obtained with oil-immersion objectives (and condensers).

Two ancillary investigations were initiated during the course of the work. In the first, the indices of refraction of the epoxy mounting medium and the major binder phases encountered were measured using the Becke method at a wavelength of 583 nm. In the second, microhardness values were measured on previously polished samples. We performed microhardness tests on each component of three representative specimens, using a commercial instrument⁶ and applying a Vickers indenter under 10 g load for 15 seconds. The hardness measurements were all made at room temperature, approximately 25°C . Due to the heterogeneous nature of the material, we made at least 10 indentations in both the epoxy and the explosive. Additionally, on the two PBX 9501 samples (molding powder and pressed piece) separate measurements were made on large single crystals and on regions dominated by binder and fine crystals, since the size of the large crystals in these samples permitted easy hardness measurement on individual crystals. Each indentation was measured from three to five times and the averages for each indentation were then averaged with the values from the other indentations to obtain a representative hardness value for the material.

Results

HMX/PBX 9501

Figure 1 shows, for reference, a reflected-light image of a pellet pressed to 7% porosity from pure commercial HMX (coarse class) devoid of binder. Contrast in the digital image is intrinsically poor and has been significantly enhanced in printing this image. The poor contrast is an expected consequence of the transparency of HMX, which

both minimizes direct reflection from the front sample surface and contributes confusing multiply-reflected signals from subsurface boundaries.

These predictable disincentives to reflected-light imaging are surprisingly mitigated in the PBX samples, and the technique proves very informative. Figure 2 shows a molding powder granule from our commercial PBX 9501, imaged in reflection with parallel polars. Visual interpretation of the image is somewhat complicated (especially for computers) by the polished epoxy mount, whose reflectivity approximates that of the HMX. For current purposes the two are distinguished by the general convexity of the coarse HMX crystals and the frequent concavity and preferential polishing of the epoxy. The image shows the specified bimodal size distribution of the HMX crystals as well as the intrusion of several pure epoxy “lakes” filling coarse voids within the granule. The fine HMX fraction is mixed with its binder and filling epoxy into a dark constituent not well resolved in this image. Finally, we note the tendency of fine HMX particles to coat the surfaces of the granule, both interior and exterior, and that this coating of fines seems to extend somewhat out into the epoxy.

Figure 3 shows a reflected light image of a similar granule now imaged at higher resolution. Here the fine HMX particles along with associated binders and fillers (dark regions in Figure 2) are resolved. In addition, we see that the coarse HMX particles aren't always single crystals and that several dark globular defects appear within the particles. These are believed to represent solvent inclusions entrapped during the growth of the crystals and now exposed on the plane of polish. Their presence is confirmed in unpolished samples dispersed in matching index media. For present purposes, they are distinguished from pull-outs by their smooth convex shapes and their dissociation from extensive cracking in the surrounding grain. These features, imaged in near-diametral planes of polish, often resemble “fairy rings”, crudely tracking parallel to the particle surface. We note further that the coarse particles are free of thin deformation twins at this point in their history.

Attempts at high resolution reflected light microscopy on HMX have not been productive to date owing to the coincidence of index values between the crystal ($1.573 < n < 1.73$, McCrone⁷) and the traditional immersion oil ($1.516 = n$), which results in unacceptably poor contrast.

Figure 4 shows a low magnification image of a piece pressed (1% porosity) from this same molding powder. In addition to the elimination of the coarse intragranular voids present in the molding powder, we see now copious fine twinning of the coarse particles. The contrast of these twins is enhanced by relief polishing in the final specimen preparation, which removes the fines (here defining the plane of focus) a few microns below the plane of the coarse particles. The plane of focus is thus within the coarse grains, which we observe to both improve contrast on the twins and degrade that of surface scratches. Finally, we note that a few angular dark patches, notably that in the fines in the upper central region, are attributable to pull-out during polishing.

Figure 5 shows a higher resolution view of the same PBX 9501 pressed piece. This image shows the accumulation of significant crack densities within the coarse grains after pressing. It also shows the “fairy ring” solvent inclusion described above, and that the ring seems to arrest the progress of twins across its crystal. Finally, we note that the twins are not straight and that they appear to interact with numerous other crystal defects, including visible voids and cracks and presumably slip lines not directly imaged here.

PBX 9502

Figure 6 shows a low magnification reflected light image of a molding powder granule from PBX 9502. It's a quite different structure in a quite different material, based on TATB rather than HMX. First, the difference in reflectivity between TATB and epoxy is much greater than that in HMX as a result of the extraordinary anisotropy of TATB (Cady⁸). Second, the granule is much less dense than the 9501 granules. Third, the

particle size distribution of the TATB grains is unimodal and comparable with the coarse fraction of HMX in 9501. Finally, within the TATB grains we observe numerous fine voids or “wormholes” characteristic of the amination chemistry of the production process.

Figure 7 shows a high resolution reflected light image of a TATB grain within the molding powder. It is first noteworthy that oil-immersion imaging with standard ($n=1.516$) oil produces acceptable contrast in bright grains of TATB. Second, the wormholes are fine, quite widely distributed, and irregular in form. Finally, the TATB particles constituting the bulk of the molding powder do appear to be single crystals.

Figure 8 shows a low magnification reflected light image of a pressed piece of PBX 9502 (3% porosity). Relief polishing, used to advantage in bimodal PBX 9501, is a nuisance here, though it does highlight the greater remanent void fraction here.

Figure 9 shows a higher magnification view of pressed 9502. We see, in addition to the wormholes remanent from the molding powder, a collection of coarse new twins. Figure 10 shows a high resolution image of a TATB grain. As in HMX, the twins are not straight, indicating that they interact with other strain sources within the grain, most likely slip bands. In contrast to HMX, two distinct systems are quite active, though their twins do not appear to interpenetrate gracefully. Figure 11 shows a high resolution image from a PBX 9502 pressed piece, this time in transmitted light. In contrast to observations in HMX, shear planes in TATB (thin twins and slip bands) appear able to penetrate the wormholes, though the wormholes, which are finer and more widely dispersed than the fairy rings, should be more potent hardeners.

Figure 12 shows a reflected light image of a sample of pressed PBX 9502 damaged by further quasistatic compression. The crack is notably branched and notably non-planar, both suggestive of toughening by localized deformation. Both intergranular and transgranular paths are evident in the image, and the transgranular routes appear far more convoluted.

X-0535

Figure 13 shows a reflected light image of an X-0535 molding powder (based on TZX explosive). In contrast to both previous materials, the TZX grains are faceted single crystals. The binder in this formulation appears to wet the grains poorly, with significant binder aggregates occasionally visible between particles. The overall density of the molding powder granule is again quite low. The TZX grains vary widely in contrast, a result of birefringence, and are sometimes twinned.

Figures 14 through 16 show images of a pressed piece of X-0535 (4% porosity). While the density of the pressing is apparently uniform, its structure is not, as evidenced by the localized rubble of fines in figure 14. Figure 15 shows, at somewhat higher resolution, a more typical grain size distribution of comminuted fine particles dispersed amongst the surviving initial particles. Several of the larger grains show cracks. A few crystals show etch figures, notably one triangle, which must be artifacts of chemical interaction with the silica/water final polish. No intragranular voids are apparent in this material.

Figure 16 shows a high resolution reflected light image of twins in a TZX grain. Again, two systems are apparent, though there's now a suggestion that they do interpenetrate. Again, the twin boundaries are not straight, indicating that they are only one of several mechanisms operable for achieving plastic strain in this material.

Mechanically Insulted PBX 9501

Figure 17 provides a schematic description of a ballistically damaged sample of PBX 9501. Here a rounded steel projectile impacted a constrained PBX sample at a speed of 127 m/sec along the path of the coarse arrow. The sample survived without detonation¹, and was eventually potted, resawn, repotted, and twice polished. Series of images were obtained from both the plan (upper arrows) and cross-sectional (right arrow) view, as shown in Figures 18 through 20. Figure 18 shows a cross section of the far field, with the

projectile incident from below at an impact point far below the region imaged. The distribution of cracks and twins is striking, again enhanced by the preferential polishing of the fines to give a plane of focus within the coarse crystals. Note the copious twinning in several coarse grains, with the twin bands inclined at ca 45 degree angles to the vertical. Note also the substantial preferred orientation of the cracks in the vertical direction.

Figures 19 and 20 are plan-view images of what remains of the impact point and the far-field. The combination of constrained compressive stress and local heating in the impact zone has produced a dense skin on that surface of the material, reminiscent of the neat HMX of figure 1, and again here in marginal contrast. Further away from the impact, crack distributions are now largely random, frequently crossing coarse crystals like slices in a pie.

Refractive Index and Hardness Data

In order to better interpret our microscopical results, we have reviewed and remeasured when necessary both the optical and mechanical properties of several of our constituents.

Refractive index data on several constituent phases are summarized in Table 1.

Phase:	Refractive index:	Reference:
b-HMX	1.589, 1.594, 1.73	McCrone (1950 ⁷)
TATB	1.45, 2.3, 3.1	Cady (1963 ⁸)
Binder 9501	1.519 +/- 0.002	Present Study
Kel-F 800	1.417 +/- 0.002	Present Study
Epoxy mount	1.571 +/- 0.002	Manufacturer's data, confirmed here

Microhardness data on several constituents are summarized in table 2.

Phase:	Hardness (kg/mm²):	95% Confidence Interval	Reference:
PBX 9501 composite	3.8	±1.2	Present Study
PBX 9502 composite	8.0	±1.4	Present Study
X0535 composite	14.7	±5.8	Present Study
β-HMX single crystal	40.3		Palmer and Field
	43.4	±7.1	Present Study
Epoxy	15.5	±2.0	Present Study

The hardness data shows considerable variability for many of the measurements. However, this is not surprising when one considers the very heterogeneous nature of the composite explosives tested. The hardness variation of the single crystal HMX is likely due to the fact that the indentations were made on potted samples where the crystal face indented and the orientation of the indentation could not easily be determined. Much less

variation in measured hardness values was observed between different indentations on the same crystal than between measurements on different crystals.

Discussion

Reflected light microscopy has proved a surprisingly useful tool for characterizing even highly transparent explosive crystals. The contrast observed in typical PBX samples is likely a consequence of two effects: differential reflectivity among phases or crystals of different indices of refraction, and preferential relief polishing of soft intercrystalline binders. The observation that setting polarizer and analyzer parallel improves the intergranular contrast while Nomarski observation under perturbed crossed polars degrades it suggests that the former mechanism is predominant. Furthermore, the bireflectance of HMX does not seem sufficient to produce acceptable contrast in the absence of low-index binder, while those of TATB and TZX do seem sufficient.

While the materials of this study were chosen for their diversity in physical properties, the similarities in their structural evolution are surprising. PBX 9501 is the most mature of the three products, with a binder system which seems to effectively wet particularly the fine particles, a designed initial particle size distribution, and an ongoing program of damage characterization. Slip, twinning, cracking, and binder creep all seem to play significant roles in the preparation of the material by pressing and in its subsequent response to deformation. The cracks observed bear rational spatial relationships to the imposed strain but do not appear to be strongly oriented to their individual crystallites. The twins, on the other hand, are always observed to be thin and parallel within any single crystal, suggesting that only one system is active.

PBX 9502 is an intermediate product in the maturity of its process technology and the extent of investigation of its mechanical properties. It is derived from a unimodal distribution of particle sizes, which requires significant plastic deformation within the particles in order to consolidate to a dense compact. Again, both slip and twinning are implicated in that plastic deformation, though now multiple twin systems are activated. Crack paths in this material show dramatic evidence of that plasticity, especially in light of the limited strains to failure observed elsewhere.

X-0535 is the least mature of these products in several structurally evident ways. Its existing binder system does not wet the explosive crystals nearly as well as the previous two systems. The crystals crack and twin during compaction, again with multiple twin systems and the evident accumulation of plastic strain.

Given these initial observations, we propose to spend the next year exploring the evolution of particle size distributions, especially in the pressing of plastic-bonded HMX composites, the spatial distribution of cracks in mechanically insulted samples, especially of HMX materials, and the redistribution of binder accompanying both deformations. Several ancillary areas require further study as well, including the elastic and microplastic properties of single crystals of the explosive phases, and their relationship to the integrated properties of the PBX composites, though these studies are complicated by the relatively low symmetries of the high explosive crystals: monoclinic β -HMX with space group⁹ $P2_1/c$, triclinic TATB¹⁰ with the second-worst allowable symmetry in P 1.

Conclusion

The microscopical examination of plastic-bonded explosives was shown to be a practical tool for gaining valuable insights into the microstructural behavior of these materials at various stages of processing (molding powder, pressed pieces, mechanically insulted pieces). Polarized light techniques for both reflected and transmitted modes were applied to three qualitatively different materials within the class of less than 8% polymeric binder and 4% porosity or less. Some improvements in polishing technique have been suggested. Future microscopical work with these and other plastic-bonded explosives is envisioned, perhaps including interferometric techniques and dynamic observation of quasistatic compaction.

¹ B. W. Asay, G.W. Laabs, B.F. Henson, D.J. Funk, "Speckle Photography During Dynamic Impact of an Energetic Material Using Laser Induced Fluorescence," *Journal of Applied Physics*, accepted Jan 1977.

² Epofix, Struers Division, Radiometer America Inc., Westlake, Ohio

³ RotoPol-25 and Pedemin-S, Struers Division, Radiometer America Inc., Westlake, Ohio

⁴ S.J.P. Palmer, J.E. Field, "The Deformation and Fracture of Beta-HMX," *Proc. R. Soc. Lond. A* 383, 399-407 (1982)

⁵ OP-Chem, Struers Division, Radiometer America Inc., Westlake, Ohio

⁶ Future Tech FM-7 MicroIndentation Hardness Tester, Struers Division, Radiometer America Inc., Westlake, Ohio

⁷ W.C. McCrone, "Crystallographic Data: Cyclotetramethylene Tetranitramine (HMX)," *Analytical Chemistry* 22, 1225-6 (1950).

⁸ H.W. Cady, "Crystallographic Data for 1,3,5-Triamino-2,4,6-trinitrobenzene", *The Microscope and Crystal Front* 14, (1), (1963).

⁹ C.S. Choi and H.P. Boutin, "A Study of the Crystal Structure of b-Cyclotetramethylene Tetranitramine by Neutron Diffraction", *Acta Cryst. B* 26, 1235-40, 1970.

¹⁰ H.H. Cady and A.C. Larson, "The Crystal Structure of 1,3,5-Triamino-2,4,6-trinitrobenzene", *Acta Cryst* 18, 485-496, 1965.

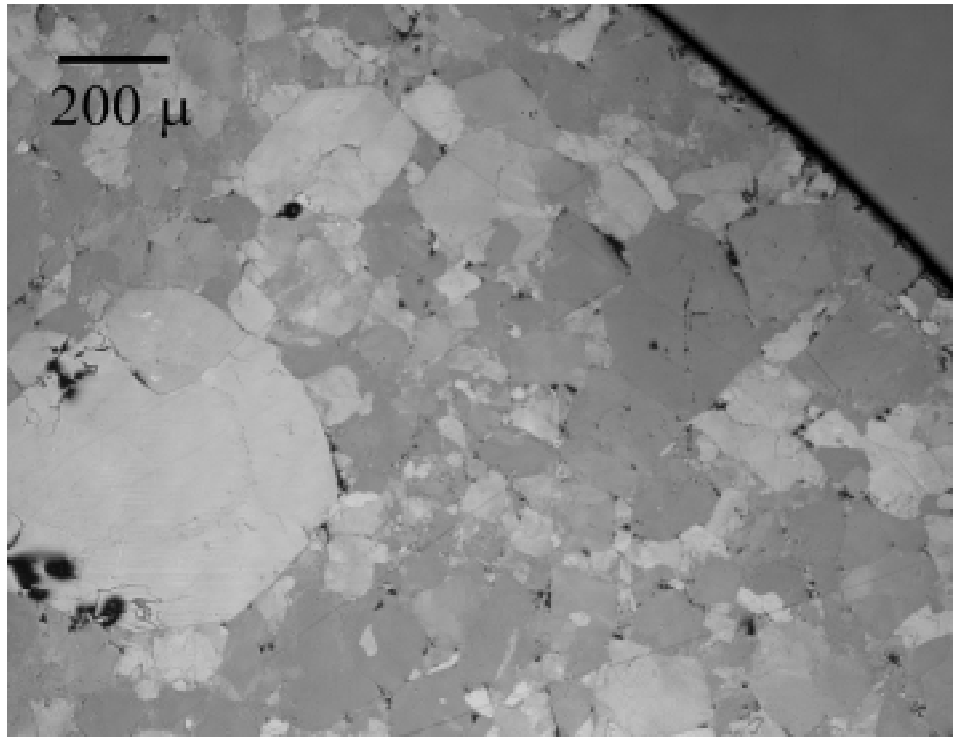


Figure1. Coarse HMX pressed to 7% porosity.

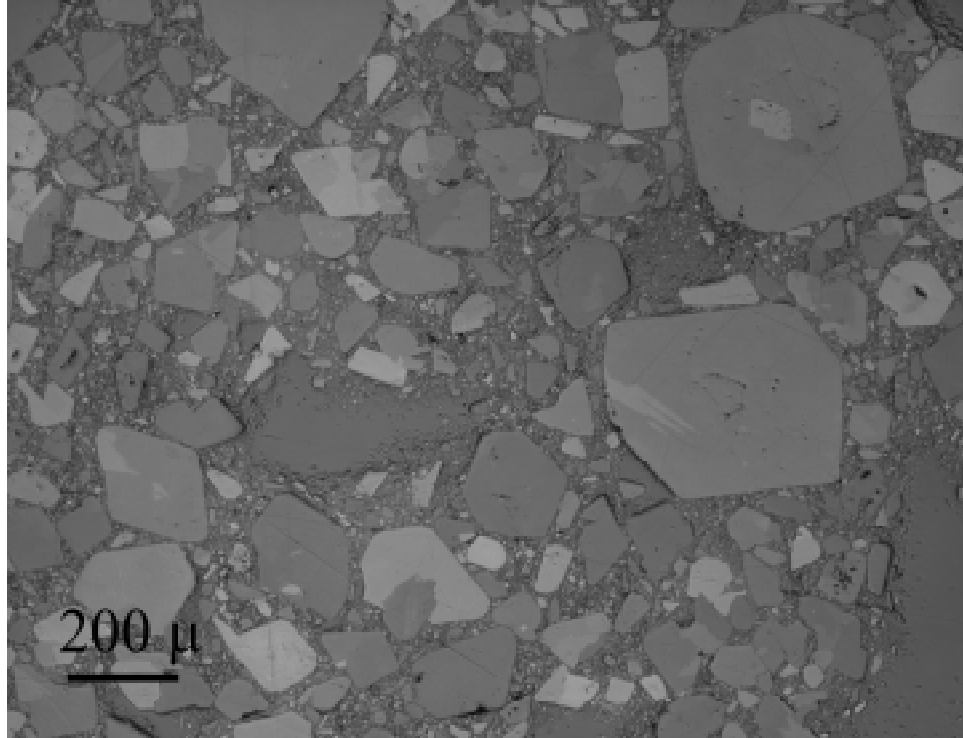


Figure 2. PBX 9501 Molding Powder Granule (low res.)

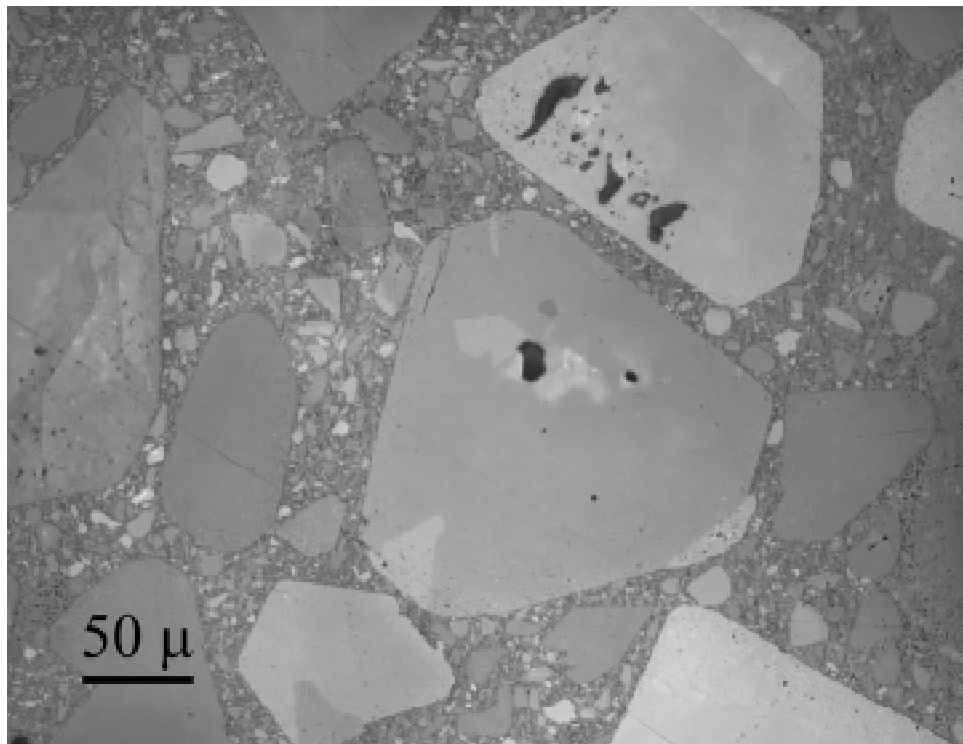


Figure 3. PBX 9501 Molding Powder Granule (med. res.)

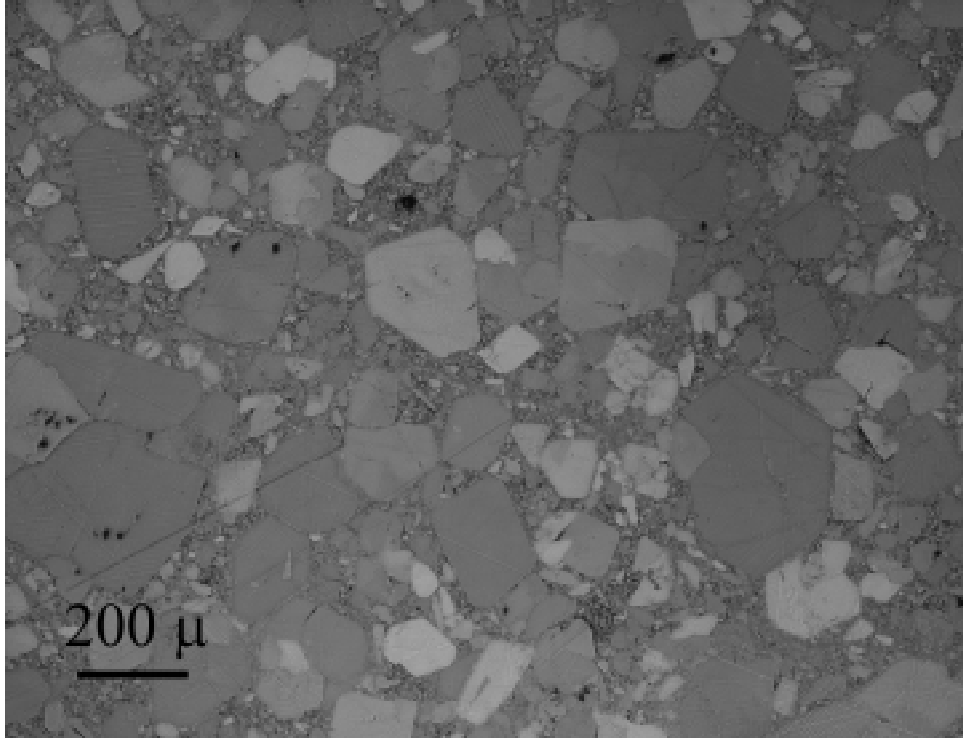


Figure 4. PBX 9501 Pressed to 1% Porosity (low res.)

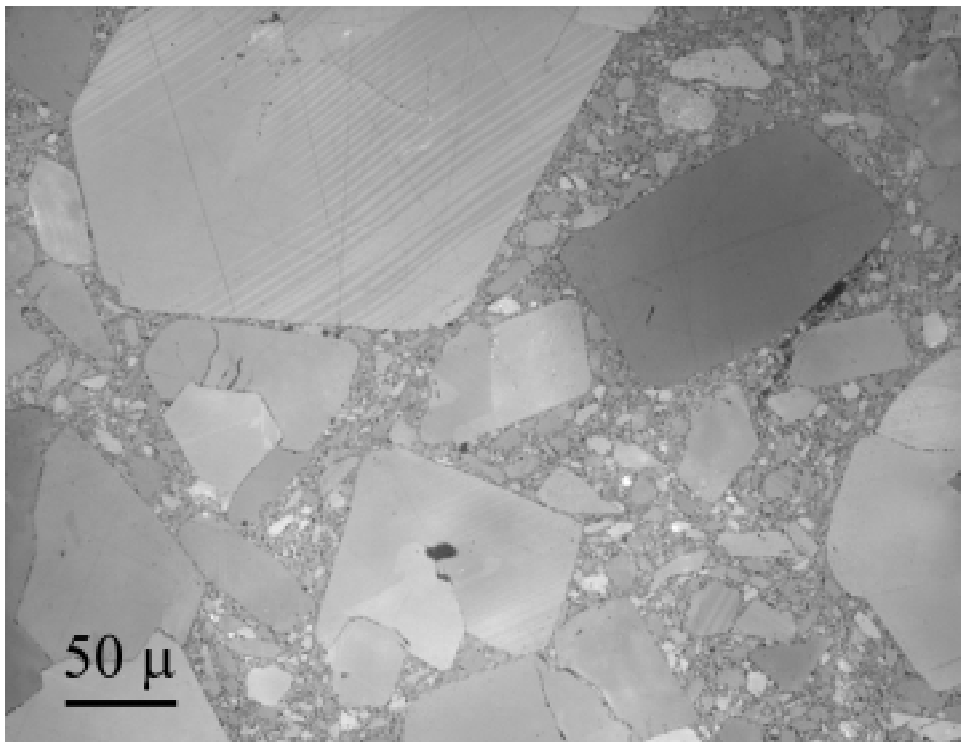


Figure 5. PBX 9501 Pressed to 1% Porosity (med. res.)

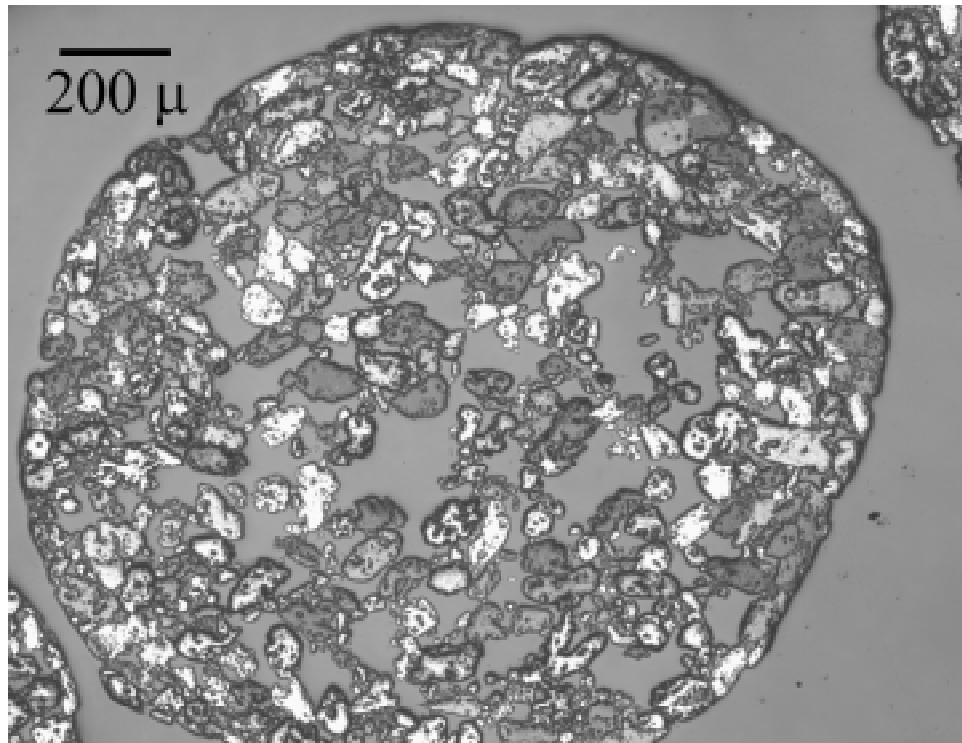


Figure 6. PBX 9502 Molding Powder Granule (med. res.)

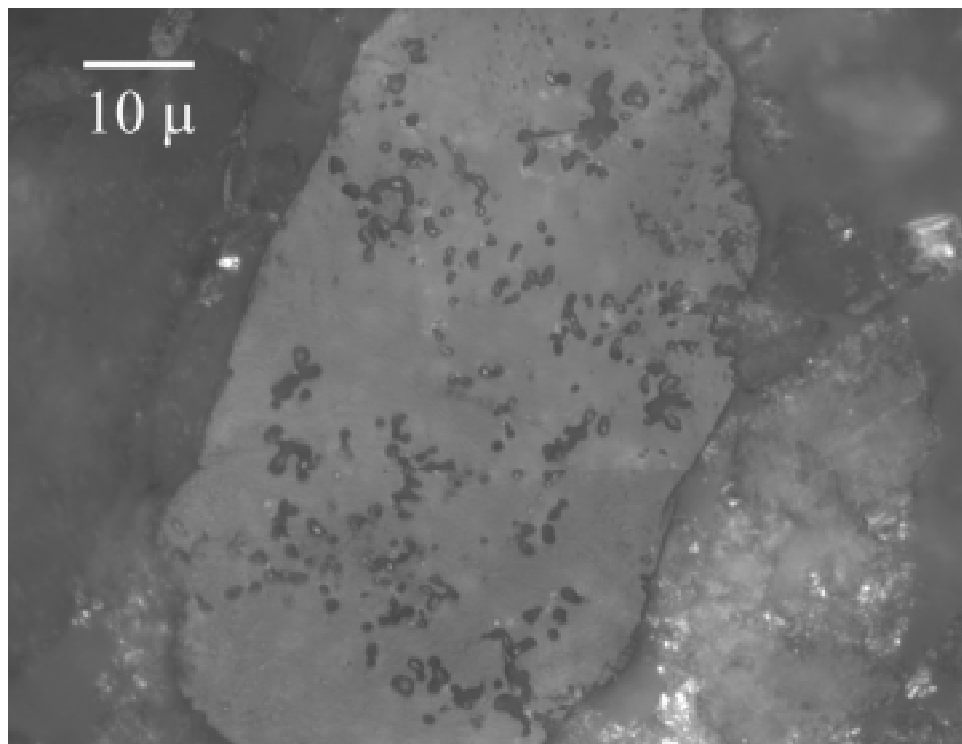


Figure 7. PBX 9502 Molding Powder Granule (high res.)



Figure 8. PBX 9502 Pressed to 3% Porosity (low res.)

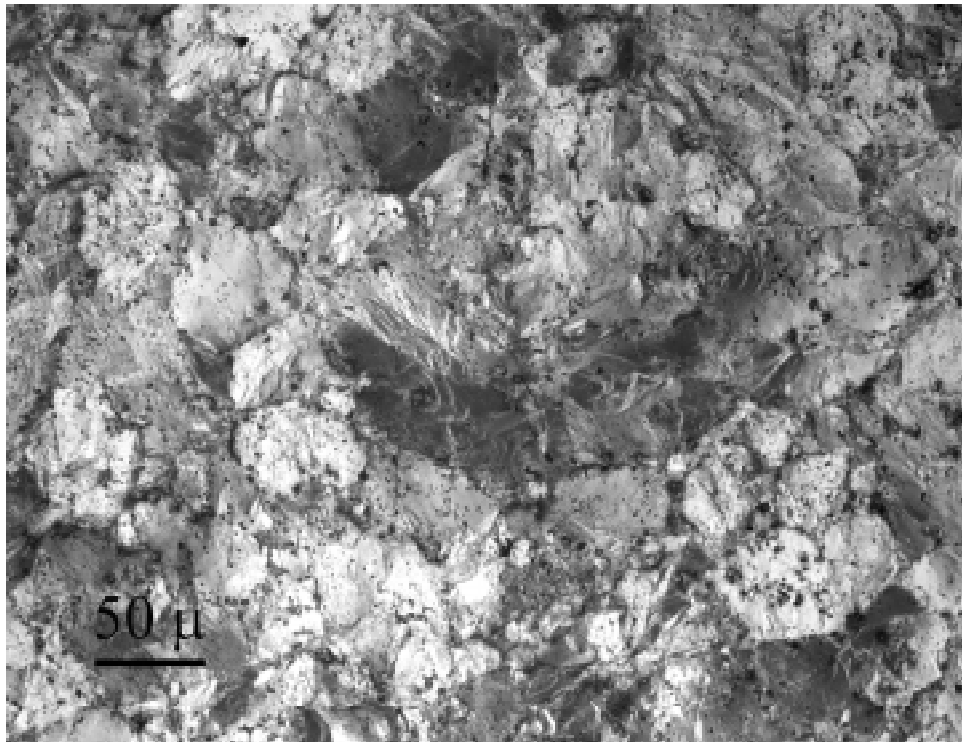


Figure 9. PBX 9502 Pressed to 3% Porosity (med. res.)

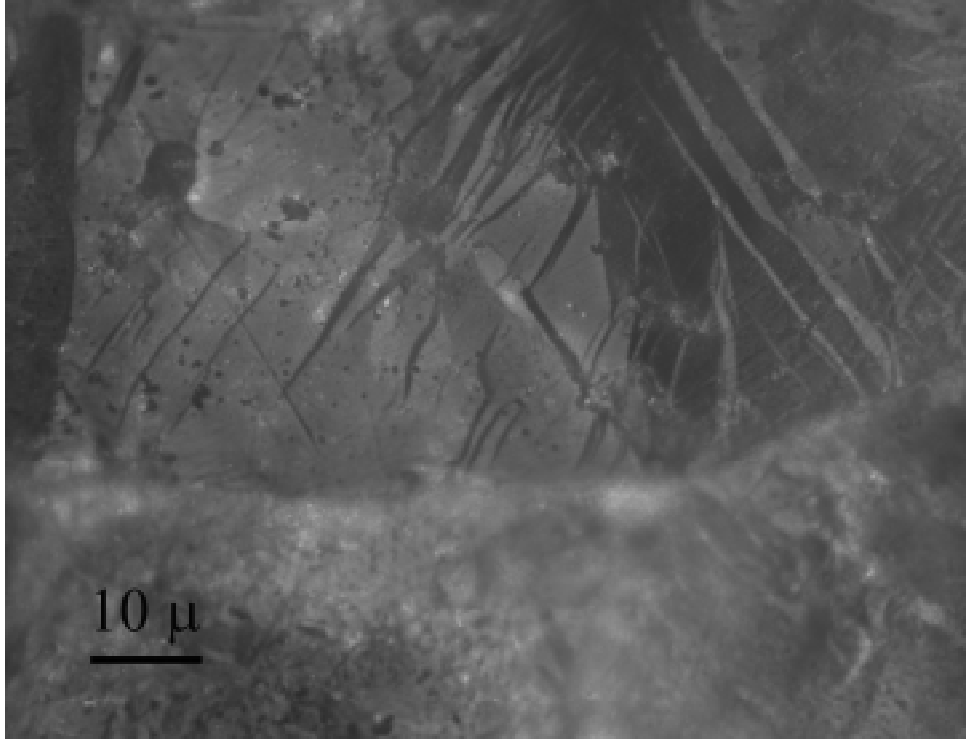


Figure 10. PBX 9502 Pressed to 3% Porosity (high res.)

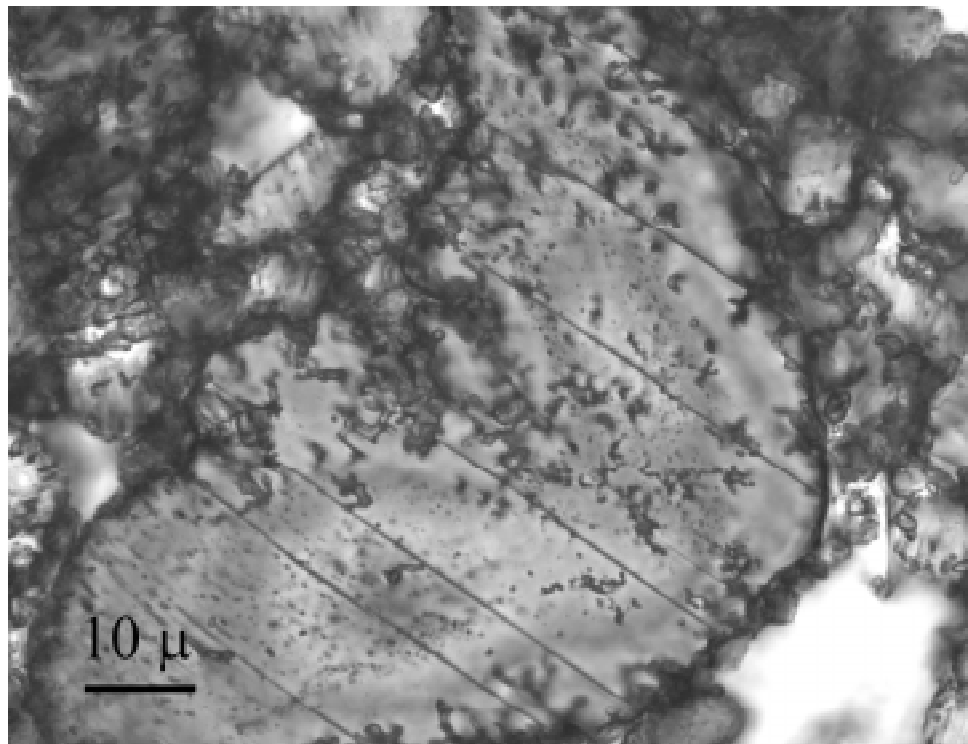


Figure 11. Thin Section PBX 9502 Pressed to 3% Porosity (high. res.)

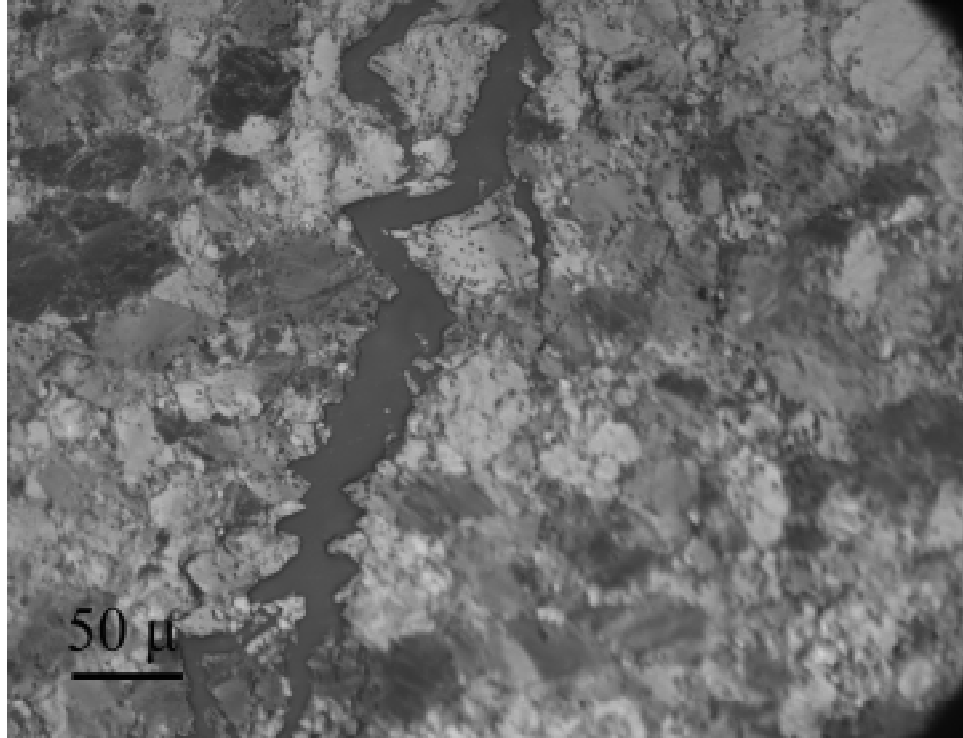


Figure 12. PBX 9502 Compressed to Failure (med. res.)

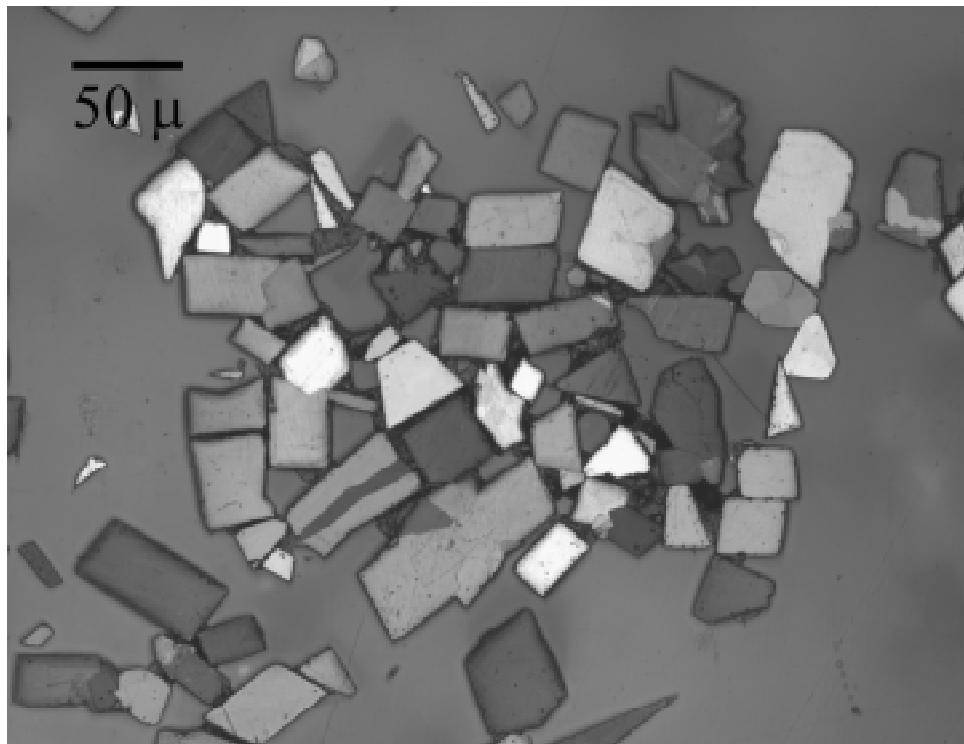


Figure 13. X-0535 Molding Powder (med. res.)

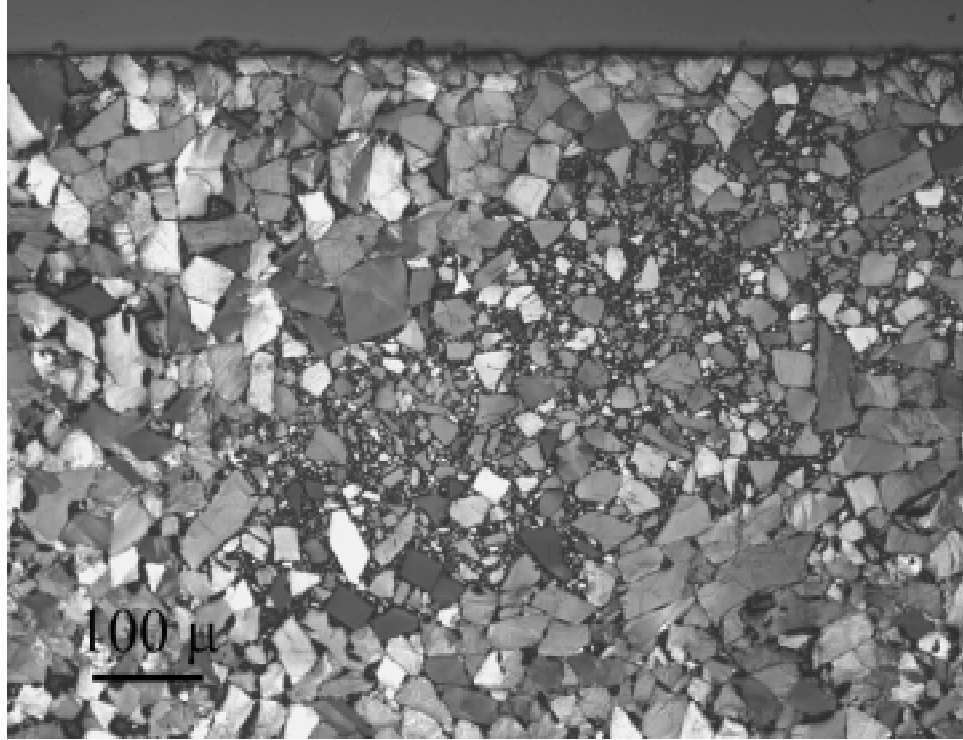


Figure 14. X-0535 Pressed to 4% Porosity (low res.)

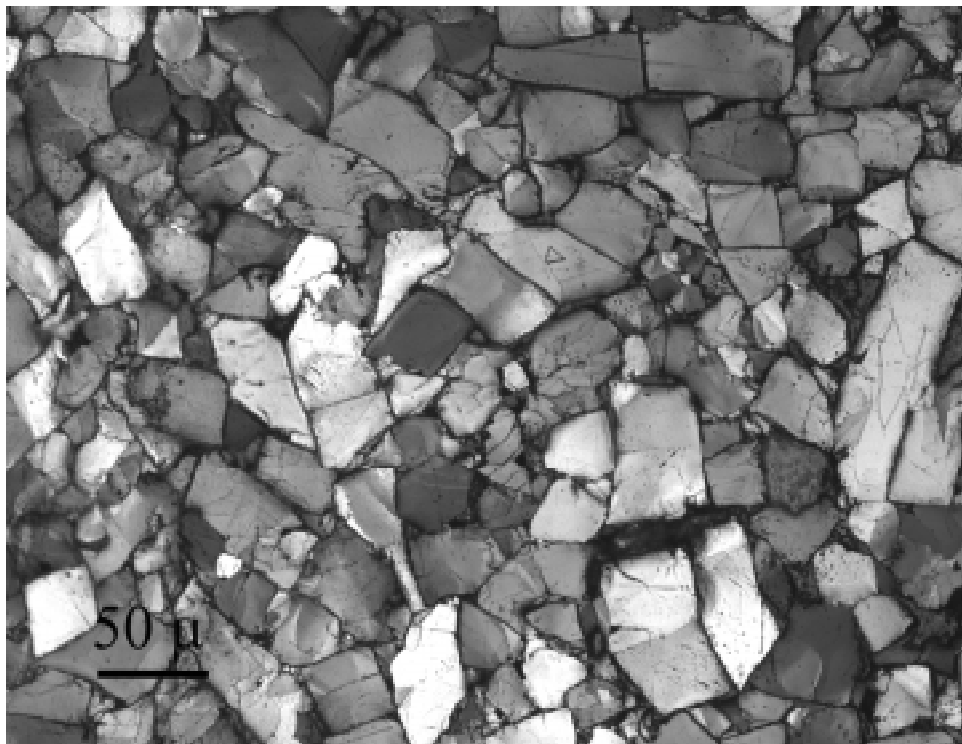


Figure 15. X-0535 Pressed to 4% Porosity (med. res.)

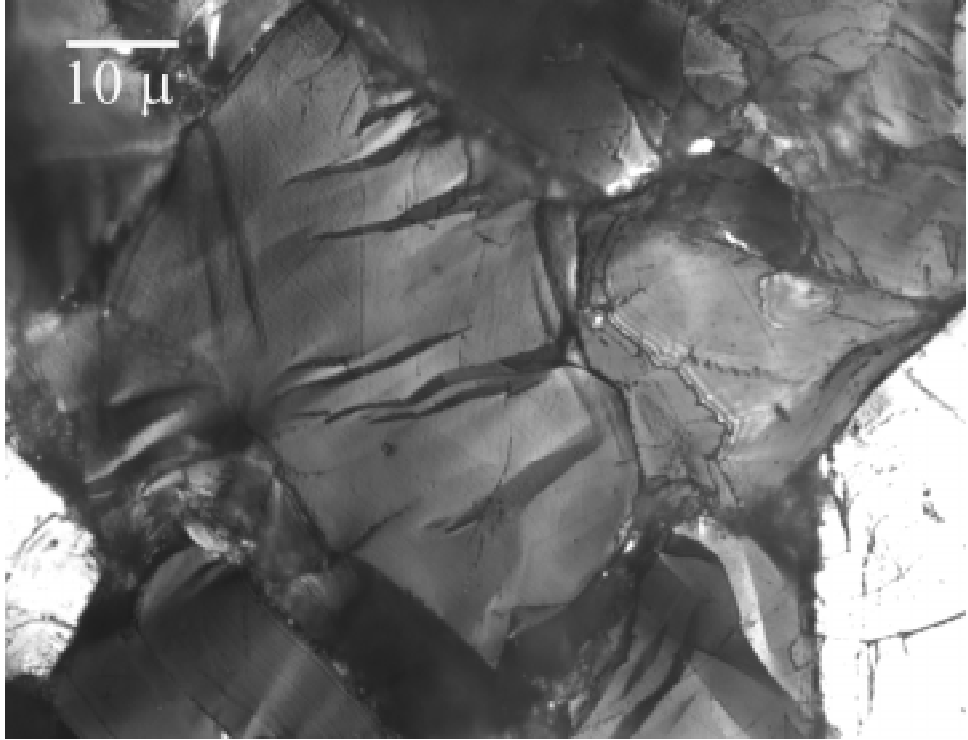


Figure 16. X-0535 Pressed to 4% Porosity (high res.)

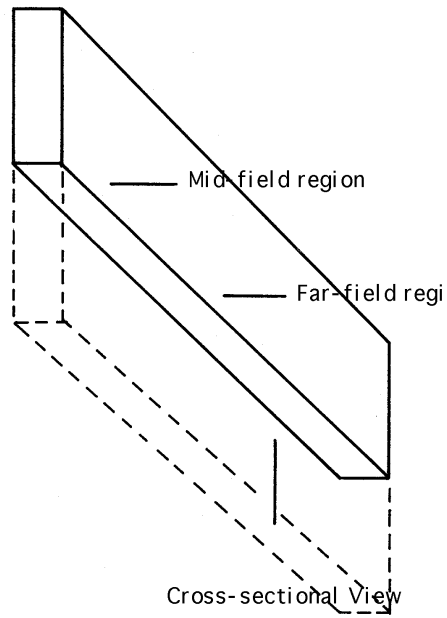


Figure 17. Schematic of Sampling from Ballistically Insulated PBX 9501.

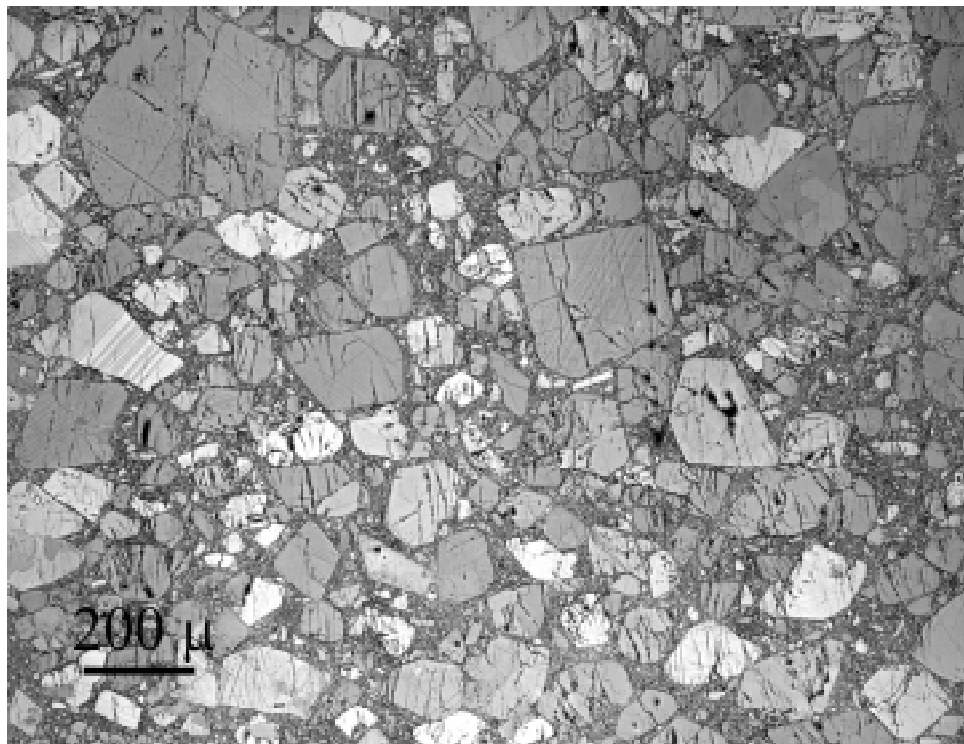


Figure 18. Far-field Region, Insulated PBX 9501, Cross-sectional View

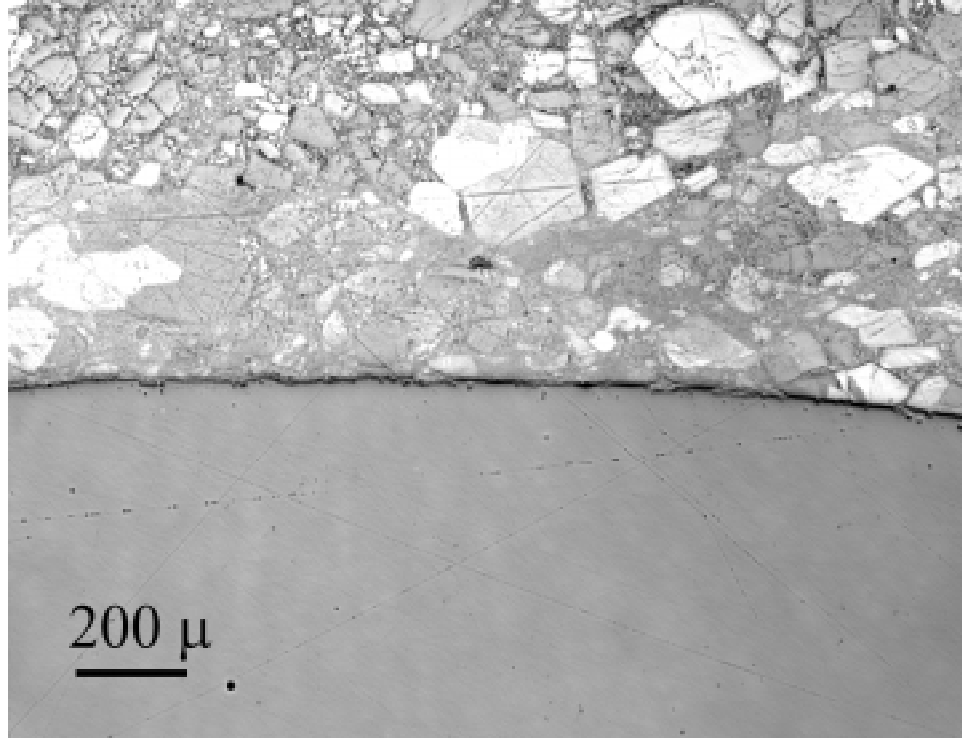


Figure 19. Impact Boundary, Insulted PBX 9501

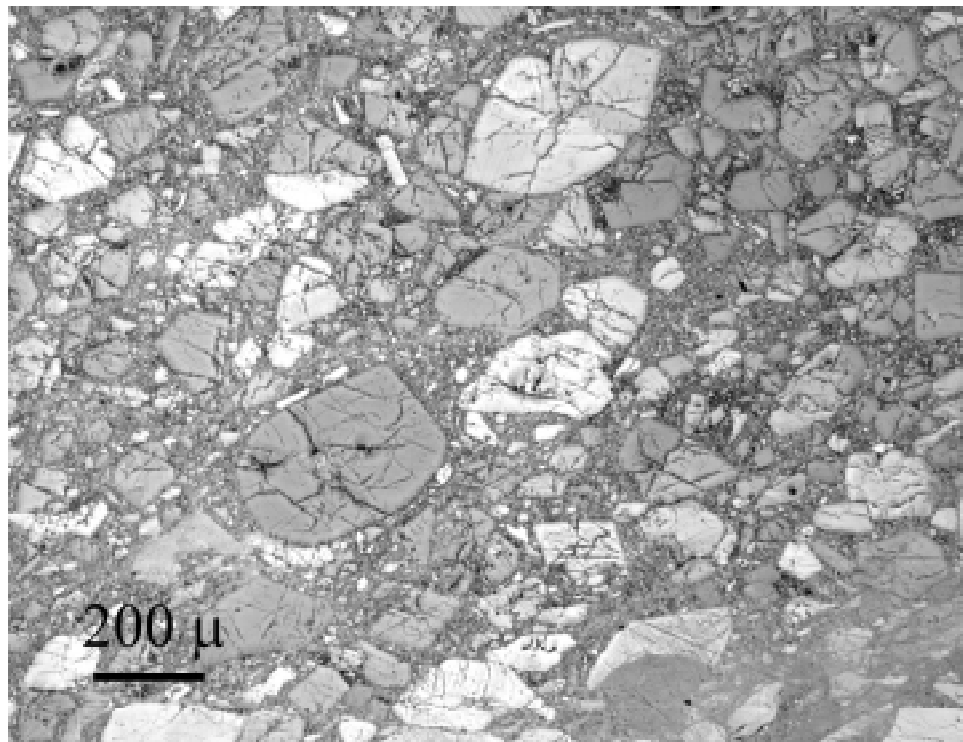


Figure 20. Mid-field Region, Insulted PBX 9501